



Cite this: *CrystEngComm*, 2021, 23, 3220  
Accepted 31st March 2021

Received 25th January 2021,  
Accepted 31st March 2021

DOI: 10.1039/d1ce00119a

rs.c.li/crystengcomm

# Cu<sub>2</sub>O nanoparticle-catalyzed synthesis of diaryl tetrazolones and investigation of their solid-state properties†

Thomas E. Reason,<sup>a</sup> Benjamin Goka,<sup>a</sup> Jeanette A. Krause,<sup>b</sup> Abelline K. Fionah,<sup>a</sup> Elsayed M. Zahran <sup>a</sup> and Sundeep Rayat <sup>\*a</sup>

An efficient and versatile method for the synthesis of 1,4-diaryl tetrazolones **1** is reported which involves C–N coupling of aryl tetrazolones **2** with aryl boronic acids **3** in the presence of Cu<sub>2</sub>O nanoparticles under an oxygen atmosphere and DMSO as solvent. The reaction tolerates a variety of electron donating and electron withdrawing substituents on both substrates and produces the desired 1,4-diaryl tetrazolones **1** in moderate to good yields. In the crystal lattice, the molecules exhibit  $\pi\cdots\pi$  stacking interactions between the adjacent layers as well as weak through-space electrostatic C–H $\cdots$ O interactions involving the pendant rings and tetrazolone carbonyl. 1-(4-Methoxyphenyl)-4-(3-tolyl)-1,4-dihydro-5H-tetrazol-5-one **1bk** and 1-(3-fluorophenyl)-4-(4-methoxyphenyl)-1,4-dihydro-5H-tetrazol-5-one **1be**, differing only in the presence of one group (methyl or fluoro), exhibited an identical pattern of noncovalent interactions in the solid-state. Hirshfeld surface analyses have also been performed to visualize intermolecular interactions.

## Introduction

Tetrazolone is an important structural motif with broad significance in medicine, agriculture, and materials science. In medicine, tetrazolone derivatives are found to be rhokinase inhibitors,<sup>1</sup> monoacylglycerol acyltransferase type 2 inhibitors,<sup>2</sup> fatty acid synthase inhibitors,<sup>3</sup> cannabinoid receptor 2 agonists,<sup>4</sup>  $\alpha_2C$ -adrenoreceptor antagonists,<sup>5</sup> and  $\beta_3$  adrenergic receptor agonists.<sup>6</sup> As a result, many tetrazolone based drugs have been patented for cardiovascular, smooth muscle, neuropathological, autoimmune, fibrotic, and inflammatory diseases as well as for treatment of cancer, obesity, diabetes and sexual dysfunction.<sup>1–6</sup> Recently, the tetrazolone scaffold has been recognized as a carboxylic acid bioisostere<sup>7</sup> as the substitution of a –COOH group in a marketed anti-hypertensive drug, with a tetrazolone ring, produced a more potent analog. In agriculture, tetrazolone is

one of the key motifs used for the design of effective fungicides,<sup>8</sup> herbicides<sup>9,10</sup> and insecticides.<sup>11,12</sup> In materials chemistry, the parent tetrazole ring has been widely utilized in the design of coordination compounds and metal organic frameworks (MOFs).<sup>13–15</sup> However, tetrazolones have not received much attention in this area. For example, eight complexes of unsubstituted tetrazolone with alkali and alkaline earth metals have been recently reported as high energy materials.<sup>16,17</sup> Two complexes of 1-methyl-5-tetrazolone with silver and palladium are known,<sup>18</sup> where the ligand binds to the metal ion at N4.

Most of the aforementioned work has focused on *N*-aryl,<sup>7</sup> *N,N*-dialkyl,<sup>19,20</sup> *N*-aryl-*N*-alkyl,<sup>6,8,9,21</sup> and *N*-aryl-*N*-triazole<sup>11</sup> derivatives of tetrazolones. On the other hand, reports on *N,N*-diarylated tetrazolones (or 1,4-diaryl tetrazolones) are limited. For instance, our group reported antiproliferative activity of 1,4-diaryl tetrazolones against L1210 leukemia and SK-BR-3 breast cancer cell lines *in vitro*.<sup>22</sup> Recently, a few *N,N*-diarylated tetrazolones have been patented for pesticidal use.<sup>23</sup> Quast and coworkers investigated the photodecomposition of 1,4-diaryl tetrazolones which results in the loss of dinitrogen and leads to the formation of benzimidazoles.<sup>24,25</sup>

The dearth of investigations on *N,N*-diarylated tetrazolones may be attributed to the lack of robust and versatile synthetic techniques to obtain these target compounds. Previously, we have reported the synthesis of these compounds through a Cu(OAc)<sub>2</sub> mediated coupling of aryl tetrazolones with aryl boronic acids in the presence of

<sup>a</sup> Department of Chemistry, Ball State University, Cooper Physical Science Building, Muncie, IN 47304-0445, USA. E-mail: srayat@bsu.edu

<sup>b</sup> Department of Chemistry, University of Cincinnati, Cincinnati, Ohio 45221-0172, USA

† Electronic supplementary information (ESI) available: Experimental procedures; TEM images of the nanoparticles; X-ray experimental description, overlaid single crystal structures as well as molecular and extended packing figures; molecular electrostatic surface potentials of **1ab**, **1ae**, **1af**, **1ag**, **1ah**, **1ai**, **1aj**, **1bd** and **1cm**; Hirshfeld surface analysis showing intermolecular interactions; <sup>1</sup>H and <sup>13</sup>C NMR spectra of all new compounds. CCDC 2052219–2052225 contain the supplementary crystallographic data for this paper. For ESI and crystallographic data in CIF or other electronic format see DOI: 10.1039/d1ce00119a

pyridine and ambient air.<sup>22</sup> However, the reaction required a stoichiometric amount of the Cu catalyst and suffered from long reaction times and poor yields. Improved synthetic methods to obtain 1,4-diaryl tetrazolones are desirable to explore the applications of these structures in various fields.

Reports on the crystal structure of tetrazolones are also limited.<sup>11,26–32</sup> Yet, knowledge of the solid-state packing of these compounds is critical due to their significance (a) in medicinal chemistry where the physical and chemical properties of an active pharmaceutical ingredient are dependent on its crystalline form,<sup>33,34</sup> as well as (2) in materials chemistry where the noncovalent interactions between the neighboring molecules are the driving force in the assembly of unorganized molecules in solution into organized supramolecular architectures in the solid state.<sup>15</sup> Thus, understanding the crystalline structure of *N,N*-diarylated tetrazolones would be valuable in designing pharmaceuticals with better efficacy and functional materials with predictable topologies.

In this article, we report an improved method to synthesize 1,4-diarylated tetrazolones which involves Cu<sub>2</sub>O nanoparticle-catalyzed aerobic oxidation of aryl tetrazolones and aryl boronic acids. We also report X-ray crystallographic analyses on select compounds in order to provide insight into the nature of the intermolecular interactions responsible for the extended packing observed in the solid-state.

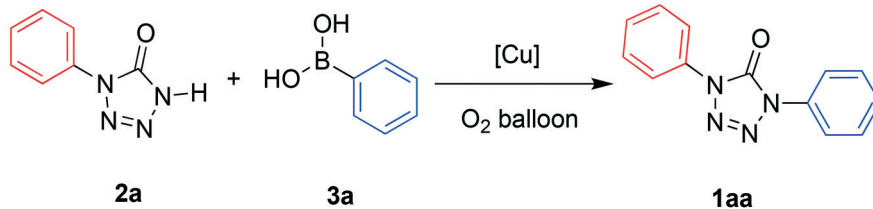
## Results and discussion

Han and coworkers have reported that Cu<sub>2</sub>O catalyzed aerobic oxidation of the aryl tetrazolones with a variety of hetero(aryl) boronates in DMSO and in the absence of a base leads to the production of 2,5-diaryl tetrazoles.<sup>35</sup> We evaluated this procedure to synthesize 1,4-diphenyl-1,4-

dihydro-5*H*-tetrazol-5-one **1aa** via the coupling of phenyl tetrazolone **2a** with phenyl boronic acid **3a** (Table 1). To our delight, **1aa** was formed in 3.5 hours and in 80% yield (entry 2), a significant improvement over the previous method<sup>22</sup> which utilized a stoichiometric amount of Cu(OAc)<sub>2</sub> and required 44 hours of reaction time to produce **1aa** in 62% (entry 1). Solvent effects on this reaction were also investigated. Previous reports on the Cu-catalyzed cross coupling of tetrazoles with boronic acids have shown that DMSO is critical for success of the reaction and it is believed that the catalytic cycle involves coordination of copper to DMSO.<sup>36</sup> The coordination of DMSO to copper moieties to enhance catalytic potential has been documented for other reactions.<sup>37,38</sup> It is reasonable to hypothesize that a similar catalytic cycle is involved in the *N*-arylation of phenyl tetrazolone **2a** with phenyl boronic acid **3a**. Replacement of DMSO with sulfolane, a structurally similar and a greener alternative, formed **1aa** in modest yield after 48 hours (entry 3). Increased reaction time and decreased yield of **1aa** in this case may be attributed to the steric bulk of the sulfolane which could hinder its coordination to copper. Substituting DMSO with ethanol, a polar protic solvent, produced only a trace amount of product after 48 hours as determined by TLC (entry 4), further emphasizing the coordination effect of DMSO.

Nanoparticle catalysts show significantly enhanced reactivity and selectivity compared to their bulk form due to large surface area to volume ratio,<sup>39–41</sup> thus prompting us to investigate the effect of the size of Cu<sub>2</sub>O nanocubes on the catalytic activity and reaction yields. Controlled low temperature hydrothermal approaches were used to prepare three different sizes of Cu<sub>2</sub>O nanostructures: 100, 300 and 800 nm.<sup>42,43</sup> Electron microscopy images were obtained to characterize the size and morphology of the Cu<sub>2</sub>O cubes prepared by the various procedures (see Fig. S1†).

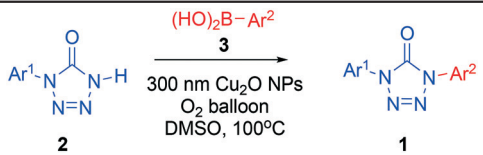
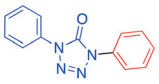
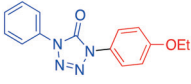
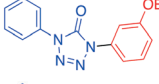
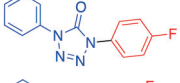
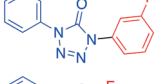
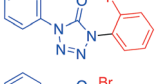
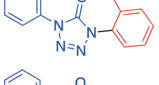
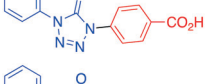
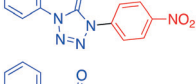
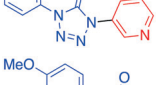
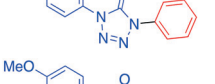
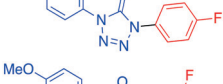
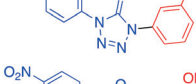
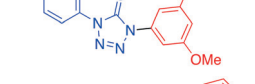
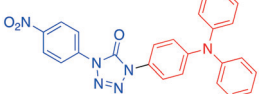
Table 1 Optimization of reaction conditions<sup>a</sup>



Entry	[Cu]	Size	mol%	Solvent	Time (h)	Yield (%)
1	Cu(OAc) <sub>2</sub> <sup>b</sup>	Amorphous	150%	CH <sub>2</sub> Cl <sub>2</sub>	44	62
2	Cu <sub>2</sub> O	Amorphous	5%	DMSO	3.5	80
3	Cu <sub>2</sub> O	Amorphous	5%	Sulfolane	48	45
4	Cu <sub>2</sub> O <sup>c</sup>	Amorphous	5%	EtOH	48	Trace <sup>e</sup>
5	Cu <sub>2</sub> O	100 nm	5%	DMSO	1	53
6	Cu <sub>2</sub> O	300 nm	5%	DMSO	2	83
7	Cu <sub>2</sub> O	800 nm	5%	DMSO	2	62
8	Cu <sub>2</sub> O	300 nm	2.5%	DMSO	1.5	46
9	Cu <sub>2</sub> O <sup>d</sup>	300 nm	5%	DMSO	24	Trace <sup>e</sup>

<sup>a</sup> Reaction conditions unless otherwise indicated: **2** (1.0 mmol), **3** (2.0 mmol), and Cu<sub>2</sub>O in DMSO (8 mL) at 100 °C. <sup>b</sup> Reaction conditions: **2** (1.5 mmol), **3** (3.0 mmol), pyridine (3.0 mmol, 2 equiv), Cu(OAc)<sub>2</sub> (2.3 mmol), molecular sieves (3 Å, 0.8 g) in DCM (30 mL) stirred at room temperature in air. <sup>c</sup> Reaction carried out at 60 °C. <sup>d</sup> Reaction carried out at room temperature. <sup>e</sup> From TLC.

**Table 2** C–N coupling of aryl tetrazolones **2** with aryl boronic acids **3**<sup>a</sup>

<div style="text-align: center;">  </div>				
Entry	Compound	Structure	Time (h)	Yield (%)
1	<b>1aa</b>		2(44 <sup>b</sup> )	83(62 <sup>b</sup> )
2	<b>1ab</b>		2	60
3	<b>1ac</b>		1.5	87
4	<b>1ad</b>		2(24 <sup>b</sup> )	81(60 <sup>b</sup> )
5	<b>1ae</b>		2(77 <sup>b</sup> )	76(21 <sup>b</sup> )
6	<b>1af</b>		72	Trace <sup>c</sup>
7	<b>1ag</b>		48(60 <sup>b</sup> )	Trace <sup>c</sup> (54 <sup>b</sup> )
8	<b>1ah</b>		4–24 <sup>d</sup>	48
9	<b>1ai</b>		4–25 <sup>d</sup>	46
10	<b>1aj</b>		24	51
11	<b>1bk</b>		2(96 <sup>b</sup> )	80(16 <sup>b</sup> )
12	<b>1bd</b>		2	79
13	<b>1be</b>		2(48 <sup>b</sup> )	80(23 <sup>b</sup> )
14	<b>1cl</b>		2.5	77
15	<b>1cm</b>		2.5	77

<sup>a</sup> Reaction conditions unless otherwise indicated: **2** (1.0 mmol), **3** (2.0 mmol), and Cu<sub>2</sub>O in DMSO (8 mL) at 100 °C. <sup>b</sup> Reaction conditions: **2** (1.5 mmol), **3** (3.0 mmol), pyridine (3.0 mmol, 2 equiv), Cu(OAc)<sub>2</sub> (2.3 mmol), molecular sieves (3 Å, 0.8 g), in DCM (30 mL) stirred at room temperature in air. <sup>c</sup> From TLC. <sup>d</sup> Exact reaction time could not be determined due to limited access to the laboratory due to COVID-19 restrictions.

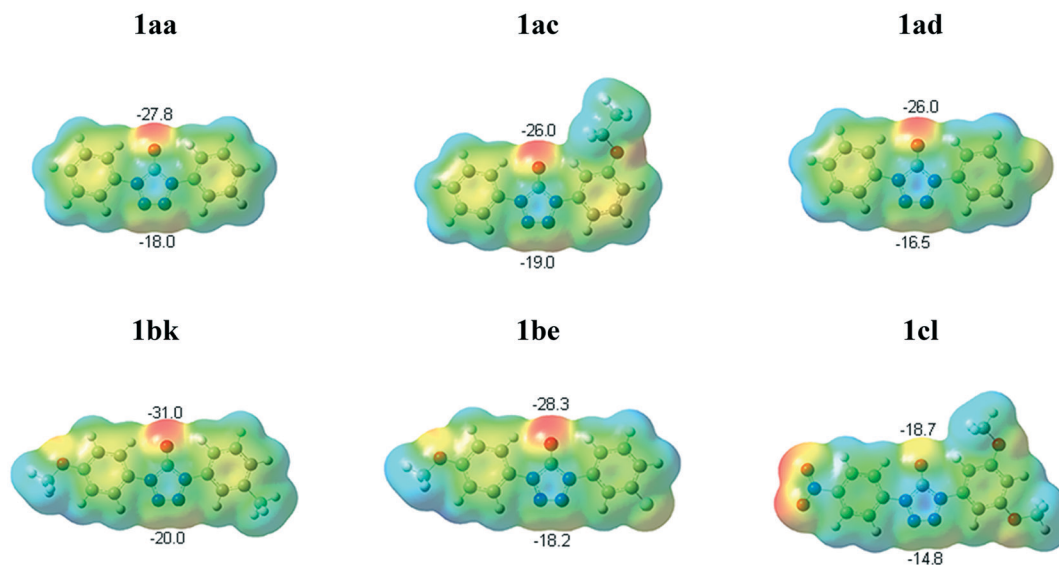


**Fig. 1** Molecular electrostatic potentials at 0.001 a.u. iso-surface of electron density for **1aa**, **1ac**, **1ad**, **1bk**, **1be** and **1cl**, calculated at M062X/6-311G\*. The MESP values of the surface minima ( $V_{s,min}$ ) at the selected points are in kcal mol<sup>-1</sup>.

The different sizes of nanoparticles studied (entries 5–7) showed a decrease in overall reaction time ( $\leq 2$  h) compared to the amorphous Cu<sub>2</sub>O (entry 2). However, only the 300 nm Cu<sub>2</sub>O nanocubes produced yields commensurate with the amorphous catalyst (entries 2 & 6), while the 100 and 800 nm nanoparticles (entries 5 & 7) resulted in decreased product yields. The reason for the limited activity of the 100 nm nanoparticles is not understood at this time. It may be due to the different oxidation state of the copper on the surface of the catalyst, however, further investigations are needed to verify this hypothesis. From these results, it was determined that 300 nm Cu<sub>2</sub>O nanoparticles would be best to use for the formation of 1,4-diaryl tetrazolones. Using the 300 nm Cu<sub>2</sub>O nanocubes, we also examined a lower catalyst loading (2.5 mol%) for coupling of **2a** and **3a**, but the yield suffered greatly compared to the meager half an hour reduction in the reaction time (entry 8). The reaction at room temperature produced only trace amounts of **1aa** after 24 h (entry 9), as indicated by TLC, which suggested that temperature plays an important role in the efficiency of this reaction. Note that Han *et al.* have shown that reaction of 5-phenyltetrazole with 4-methylphenyl boronic acid in the absence of Cu<sub>2</sub>O catalyst

did not produce any product.<sup>35</sup> We expected a similar outcome for the reaction of **2a** with **3a**.

After the optimized conditions were determined, we set out to examine the scope of this C–N coupling with a variety of aryl tetrazolones **2** and aryl boronic acids **3** (Table 2). Phenyl tetrazolone **2a** reacted with aryl boronic acids substituted with an electron-donating ethoxy group at the *para* and *meta* positions to give **1ab** and **1ac** in 60% and 87% yield, respectively (entries 2 and 3). The coupling reaction also tolerated the presence of a weakly-deactivating fluoro group at the *para* and *meta* positions of the phenylboronic acid and produced **1ad** and **1ae** in excellent yields (entries 3 and 4). Note that these compounds were prepared in 60% and 21% yields, respectively, after many hours using the Cu(OAc)<sub>2</sub> method.<sup>22</sup> In comparison, the *ortho* substitution of the weakly-deactivating fluoro and bromo groups produced only trace amounts of tetrazolones **1af** and **1ag** after several hours, which may be attributed to steric hindrance encountered during coordination to copper in the catalytic cycle (entries 6 and 7). It is worth noting that **1ag** can be produced in 54% yield after 60 h using the Cu(OAc)<sub>2</sub> method.<sup>22</sup> The presence of moderately and strongly electron-withdrawing carboxylic acid

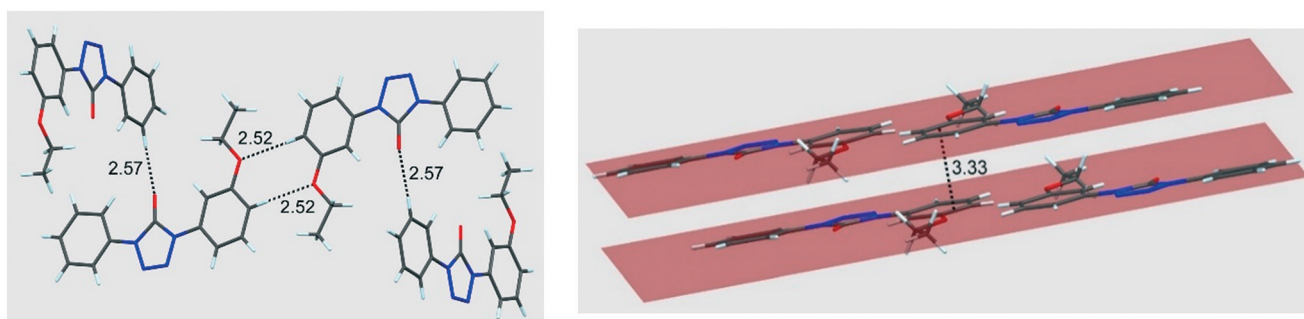


**Fig. 2** Left: C–H⋯O intermolecular interactions in the crystal lattice of **1ac**; right: interplanar stacking arrangement.

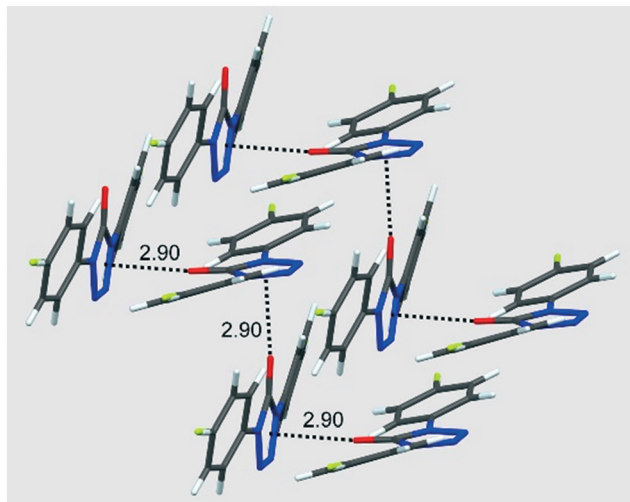


Fig. 3 Interplanar interactions in the crystal lattice of **1ad**.

and nitro groups required prolonged reaction times and a messy extraction that led to loss of the product and thus, reduced yields of **1ah** and **1ai**, respectively (46–48%, entries 8 and 9). The versatility of this method was also examined for a heteroaryl boronic acid, specifically the 3-pyridyl boronic acid which produced **1aj** in moderate yield (51%, entry 10) upon reaction with **2a** after 24 h.

Next, we examined the *N*-arylation of substituted phenyl tetrazolones with boronic acids. Our work revealed that **2b** substituted with an electron-donating *para* methoxy group underwent coupling with phenyl boronic acid substituted with weakly activating (*m*-Me) and deactivating groups (*m*-F and *p*-F) to give the corresponding 1,4-diaryl tetrazolones **1bk**, **1bd** and **1be** in 80% yield (entries 11–13). Similarly, the reaction of phenyl tetrazolone **2c** incorporating an electron-withdrawing nitro group with 3,5-dimethoxyphenyl- and (4-(diphenylamino)phenyl) boronic acids **3l** and **3m**, respectively, was also successful and afforded both **1cl** and **1cm** in 77% yield (entries 14 and 15).

### Electrostatic potential calculations

We were successful in obtaining single crystals of six of the synthesized compounds which includes **1aa**, **1ac**, **1ad**, **1bk**, **1be** and **1cl**. To understand the intermolecular interactions in the solid-state of these compounds, the structures were optimized at the M062X/6-311G\* level of theory using Gaussian 09 package of programs.<sup>44</sup> The molecular electrostatic potentials (MESP) plots and surface minima ( $V_{s,min}$ ) were calculated and visualized using GaussView.<sup>45</sup> The MESP analysis shows that the greatest degree of negative charge (red region) is concentrated at the carbonyl oxygen and to a lesser extent near the N=N unit of the tetrazolone ring in these molecules, while positive charge (blue region) is concentrated at the centroid of the tetrazolone (Fig. 1).

### X-ray crystallography

The molecular structure diagrams and crystal data refinement details of **1aa**, **1ac**, **1ad**, **1bk**, **1be** and **1cl** are given in Fig. S3–S9 and Tables S1–S7.† **1aa** crystallized from dichloromethane in the tetragonal  $P4_1$  space group as six independent molecules in the asymmetric unit. In contrast, **1ac**, **1ad**, **1bk**, **1be** and **1cl** crystallized as one independent molecule in the more common monoclinic or orthorhombic crystal systems. **1be** crystallized as either a monoclinic C-centered polymorph from methanol (**1be<sub>MeOH</sub>**) or a primitive monoclinic polymorph from acetonitrile (**1be<sub>MeCN</sub>**). As expected, the individual rings in all the complexes are planar. The **1aa** pendant phenyl rings vary in dihedral angle relative to the central tetrazolone core (0.7(2)–19.7(2)°) with most molecules showing a slight twist in the position of the phenyl rings with respect to each other rather than a more planar or bowed molecular backbone (Fig. S3†). The molecular structure of **1ac** obtained in acetonitrile, shows small deviations from planarity, 2.43(8)° and 2.87(8)°, between the central ring and the substituents, giving the molecular backbone a planar geometry (Fig. S4†). **1ad** obtained from methanol crystallizes in the centrosymmetric

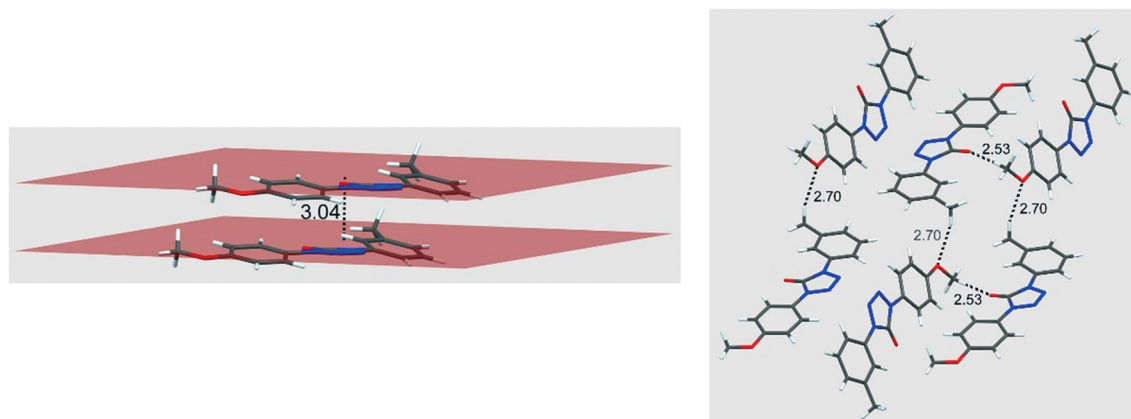


Fig. 4 Interplanar (left) and intermolecular interactions (right) between molecules of **1bk** in the crystalline lattice.



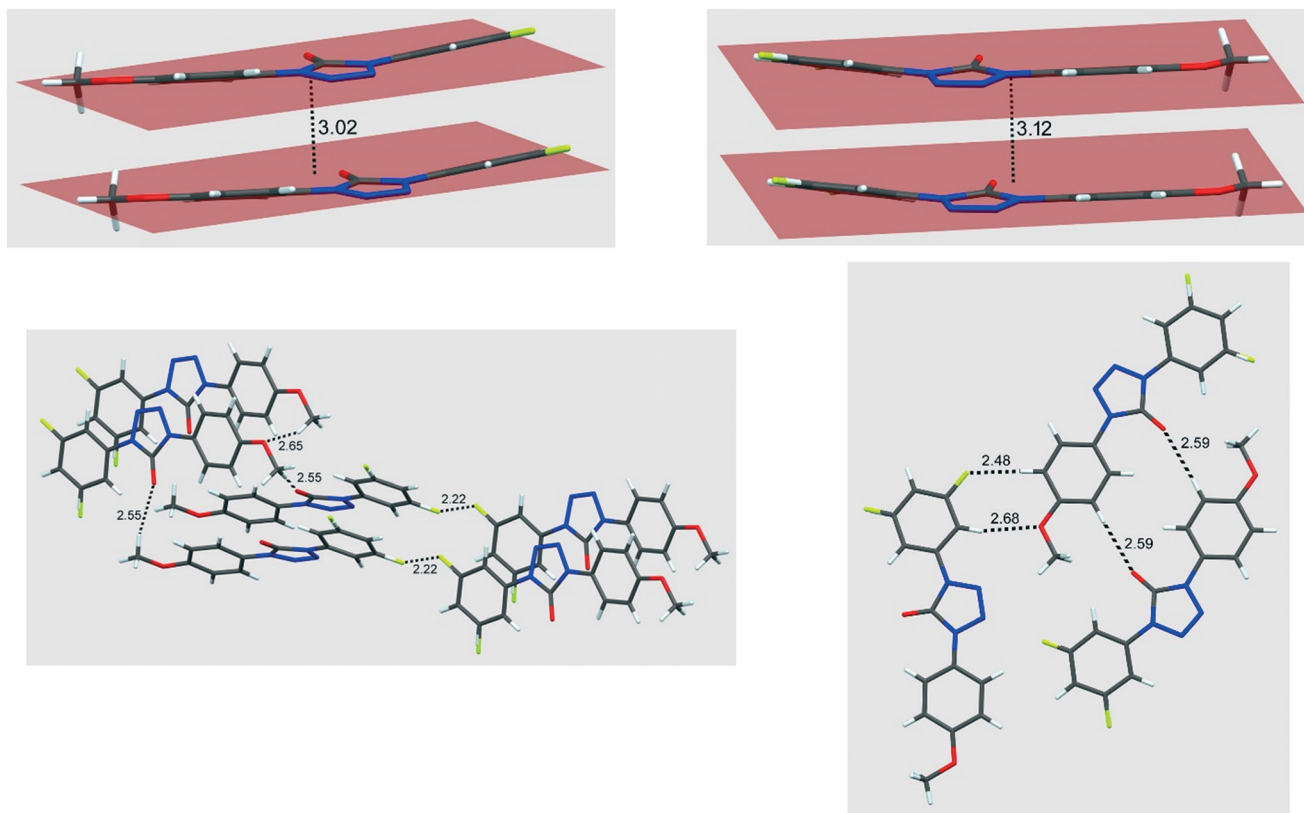


Fig. 5 Comparison of the interplanar separations (top) and C-H...O intermolecular interactions (bottom) for the polymorphs **1be**<sub>MeOH</sub> (left) and **1be**<sub>MeCN</sub> (right).

space group *Pnma* with a slightly bowed arrangement between the central heterocycle and the pendant aryl rings (dihedral angle = 15.79(6)°) (Fig. S5†). A slight twisting adopted by the peripheral rings relative to each other is

observed in **1bk** and both polymorphs of **1be** (Fig. S6–S8†) with dihedral angles clustered about 13–15° while **1cl** (Fig. S9†) shows more variation (8.9(1) and 17.1(1)°). All single crystal structures were overlayed that further show that the molecules exhibit different ring orientations associated with the pendant phenyl or substituted aryl moieties that can be described as twisting or bowing relative to the tetrazolone ring (Fig. S10†).

While the molecular structures of these complexes are rather straightforward, of interest are the extended stacking and intermolecular interactions. Examination of the extended packing structure of **1aa** revealed a layered stacking motif along the *c*-axis with varying tilt angles between the planes, however no identifiable structure-directing noncovalent interactions were observed. Inspection of the unit cell of **1ac**, revealed weak electrostatic C-H...O interactions involving an aromatic C-H of the 3-ethoxyphenyl moiety with the oxygen of a neighboring ethoxy group (2.52 Å) as well as the C-H of the phenyl group with the oxygen of a neighboring tetrazolone ring (2.57 Å). An overall slipped  $\pi$ - $\pi$  interaction between adjacent layers is observed with a 3.33 Å distance between the stacked planes and a long distance (>4 Å) between tetrazolone centroids (Fig. 2).

As deduced from the calculations, molecules **1ad**, **1bk** and **1be** pack by utilizing the electrostatic interaction between the positive and negative regions of the heterocycle. The negative

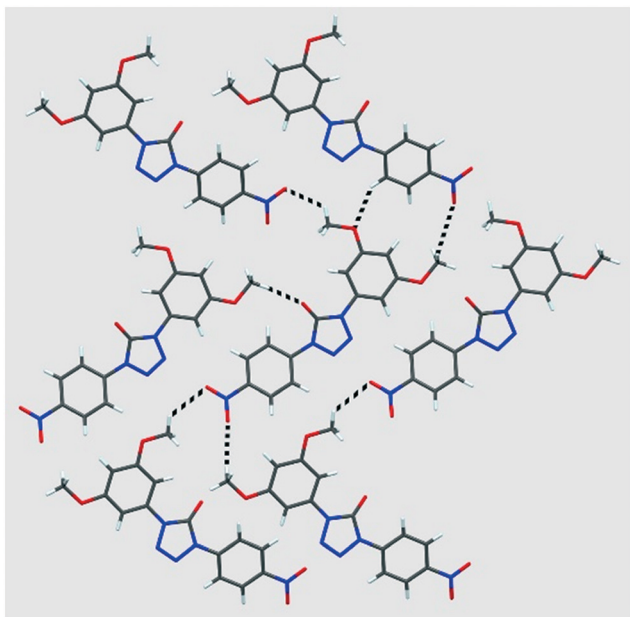


Fig. 6 C-H...O interactions (distances in the 2.5–2.7 Å range) present between molecules in the crystalline lattice of **1cl**.

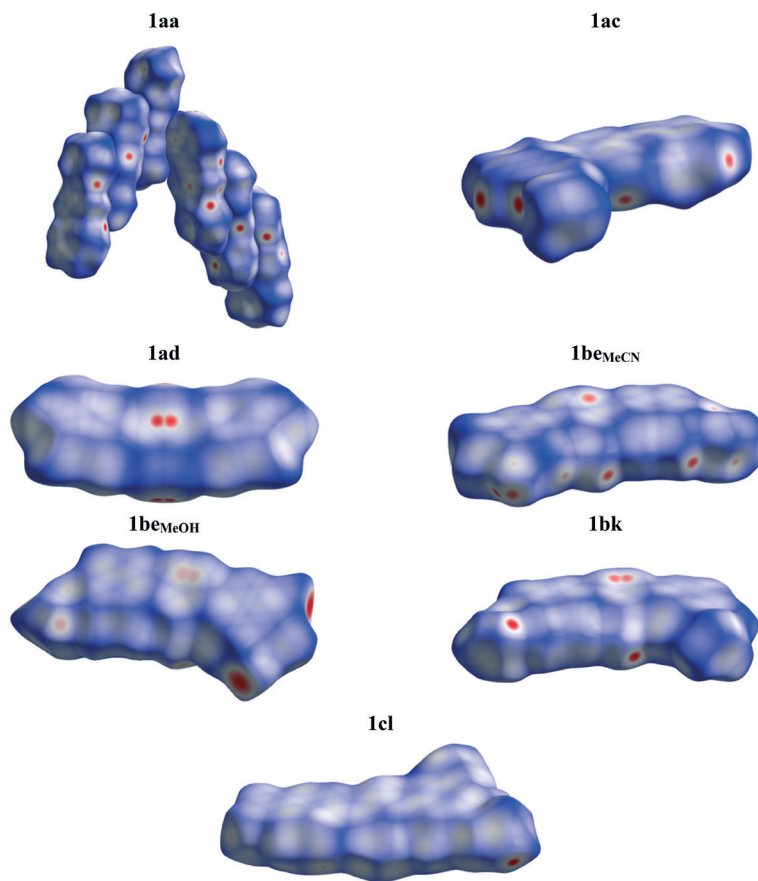


Fig. 7 Hirshfeld surface maps of **1aa**, **1ac**, **1ad**, **1be<sub>MeCN</sub>**, **1be<sub>MeOH</sub>**, **1bk** and **1cl**. Close contacts are represented as red spots.

Table 3 Hirshfeld surface analysis. Percent contribution to surface area contacts<sup>a</sup>

Molecule	O⋯H	N⋯H	C⋯C	C⋯N	C⋯O	F⋯H	F⋯N
<b>1aa 1</b>	5.4	17.7	5.0	—	—	—	—
<b>1aa 2</b>	8.6	13.6	4.6	—	—	—	—
<b>1aa 3</b>	8.4	13.5	5.5	—	—	—	—
<b>1aa 4</b>	7.7	15.1	5.0	—	—	—	—
<b>1aa 5</b>	6.8	16.0	5.2	—	—	—	—
<b>1aa 6</b>	8.4	14.9	4.9	—	—	—	—
<b>1ac</b>	9.8	10.2	5.0	—	—	—	—
<b>1ad</b>	—	2.7	1.7	—	—	—	—
<b>1be<sub>MeCN</sub></b>	12.2	6.0	9.2	3.7	—	15.4	4.4
<b>1be<sub>MeOH</sub></b>	12.1	4.7	—	2.9	13.6	—	—
<b>1bk</b>	11.7	4.3	—	2.7	—	—	—
<b>1cl</b>	30.9	5.6	—	—	—	—	—

<sup>a</sup> Contacts are given as inversion percentages. A dash indicates this is not a significant contribution to the strong interactions in a given molecule.

potential encompassing the carbonyl oxygen of **1ad** is attracted to the positive potential at the center of the tetrazolone, a C=O⋯N<sub>4</sub>C<sub>centroid</sub> interaction distance of 2.90 Å is observed giving rise to a staircase motif in the solid state (Fig. 3).

**1bk** exhibits a  $\pi$ - $\pi$  stacking motif with a least squares distance of 3.04 Å, consistent with other complexes in this study (Fig. 4). While the extended packing geometry may

approximate a herringbone motif, the individual stacks support weak C-H⋯O interactions between neighboring methyl groups and either a methoxy or carbonyl oxygen atom (C-H<sub>Me</sub>⋯O<sub>OMe</sub> = 2.70 Å, C-H<sub>OMe</sub>⋯O=C = 2.53 Å) rather than with the tetrazolone heterocyclic N<sub>4</sub>C core.

Two polymorphs of **1be** result from methanol (**1be<sub>MeOH</sub>**) or acetonitrile (**1be<sub>MeCN</sub>**) crystallization (Fig. 5). The noncovalent interactions observed for **1be<sub>MeOH</sub>** approximate

those of **1bk**, namely a  $\pi$ - $\pi$  stacking of 3.02 Å between the adjacent stacked planes and individual stacks held *via* C-H $\cdots$ F interactions involving the pendant aromatic rings. A somewhat longer,  $\pi$ - $\pi$  stacking interaction, 3.12 Å, is seen for **1be<sub>MeCN</sub>** with a tetrazolone N<sub>4</sub>C<sub>centroid</sub> $\cdots$ N<sub>4</sub>C<sub>centroid</sub> distance of 3.84 Å indicative of a very weak, inefficient electrostatic attraction. One can conclude that the placement of the molecules is dictated by the C-H $\cdots$ O and C-H $\cdots$ F interactions rather than tetrazolone ring interactions for both crystals of **1be**.

**1cl** adopts a slipped pattern that has a large stacking distance and tetrazolone centroid-to-centroid ring separation (3.27 Å and 3.90 Å, respectively), reminiscent of distances observed in **1ac**. This presumably is due to the steric requirements of two -OMe substituents on one of the rings as well as the twisted, non-planarity of the molecular backbone. Each molecule interacts with six neighboring molecules (Fig. 6) *via* through-space interactions of the type (1) C-H<sub>methoxy</sub> $\cdots$ O=C, (2) C-H<sub>methoxy</sub> $\cdots$ O<sub>nitro</sub> and (3) the aromatic C-H of a nitrophenyl ring with a methoxy oxygen (Fig. 6). These C-H $\cdots$ O interaction distances fall in a narrow 2.5–2.7 Å range indicative of similarly weak electrostatic forces influencing the packing geometry of the molecules in the lattice.

### Hirshfeld surface analysis

Hirshfeld surface analysis<sup>46</sup> of the structures of **1aa**, **1ac**, **1ad**, **1be<sub>MeCN</sub>**, **1be<sub>MeOH</sub>**, **1bk** and **1cl** revealed that predominantly surface contacts are typical van der Waals interactions. As might be expected, the majority are H $\cdots$ H contacts and will not be discussed further. Inspection of the surfaces of the molecules showed several regions on each molecule with significant, or less notable contacts (Fig. 7). These contact regions, highlighted as “red” spots on the Hirshfeld surface map, are mainly between aromatic hydrogen atoms and either oxygen or nitrogen atoms (Table 3). Other significant contacts were between tetrazole nitrogen atoms and carbon atoms on neighboring molecules. For the six independent molecules in **1aa**, C $\cdots$ C intermolecular contacts also showed signs of close approach. This is not unexpected given the  $\pi$ -stacking present in the lattice. This is also true for **1ac** and **1be<sub>MeCN</sub>**. However, **1be<sub>MeOH</sub>** did not show any significant C $\cdots$ C interactions. Similarly, **1ad**, **1bk** and **1cl** had no dominant C $\cdots$ C contacts. Surprisingly, the surface map for **1cl** was relatively devoid of any significant interactions. For the fluorinated compounds **1be<sub>MeCN</sub>** and **1be<sub>MeOH</sub>**, fluorine impacts the Hirshfeld surface and plays a role in many of the very close contacts observed in these two polymorphs (Fig. 7). Figures depicting the molecules surrounding the core molecule or molecules that contribute to these interactions can be found in the ESI† Fig. S11–S17.

## Conclusions

We have reported an improved method for the synthesis of 1,4-diaryltetrazolones **1** *via* C–N coupling of aryl tetrazolones

**2** and aryl boronic acids **3** in the presence of Cu<sub>2</sub>O nanoparticles under an oxygen atmosphere in DMSO as a solvent. This protocol provides substantial improvement over the previous method<sup>22</sup> as it uses relatively low catalyst loading, does not involve a base, requires short reaction times and produces higher yields. The reaction is generally insensitive to the nature and position of the substituents on the aryl tetrazolone or boronic acid, except in the case of *ortho* substituted aryl boronic acids where only a trace product was observed, possibly due to the steric hindrance encountered in coordination to Cu during the catalytic cycle.<sup>36</sup> Due to the relatively mild conditions, this method may be explored for its suitability in the formation of C–N bonds using other N–H containing motifs such as amines, amides, imidazoles, and indoles.

Furthermore, this is the first study that reports X-ray crystal structure analyses of 1,4-diaryltetrazolones **1**. Our work revealed the presence of  $\pi$  $\cdots$  $\pi$  stacking interactions between the adjacent layers in five of the seven structures. The assembly of molecules is further directed by weak electrostatic C–H $\cdots$ O interactions involving the neighboring pendant rings as well as the tetrazolone carbonyl and the pendant rings. Single crystals of **1bk** and **1be<sub>MeOH</sub>**, differing only in the presence of a *p*-methyl or *p*-fluoro group, respectively, displayed an identical pattern of noncovalent interactions in the solid-state. In the case of **1be<sub>MeCN</sub>** and **1be<sub>MeOH</sub>**, Hirshfeld surface analyses showed that fluorine plays a role in many of the very close contacts observed in these two polymorphs. We believe that the knowledge gained from this work, would stimulate further investigations on the crystal packing of this important class of compounds with potential to impact a variety of fields including medicinal, agricultural and materials chemistry.

## Conflicts of interest

There are no conflicts to declare.

## Acknowledgements

T. E. R. is grateful to the Ball State Honors College for the Undergraduate Honors Fellowship. Crystallographic data for **1aa**, **1ac**, **1bk**, and **1be<sub>MeCN</sub>** and **1cl** were collected through the SCrALS (Service Crystallography at Advanced Light Source) program at Beamline 12.2.1 at the Advanced Light Source, Lawrence Berkeley National Laboratory supported by the U.S. Department of Energy, Office of Energy Sciences Materials Sciences Division, under the contract DE-AC02-05CH11231. Crystal structure data for **1ad**, and **1be<sub>MeOH</sub>** were collected at the University of Cincinnati on a D8 Venture diffractometer funded through NSF-MRI grant CHE-1625737. Mass spectrometric data were obtained on a Thermo Fisher LTQ XL supported by NSF-MRI grant under CHE-1531851. Acknowledgement is also made to the Donors of the American Chemical Society Petroleum Research Fund for the partial support of this



research (ACS PRF # 61125-UR3). Computational work was performed on the Beowulf cluster supported by NSF-MRI grant CNS-1726017 and Ball State University. We acknowledge Dr. Allen G. Oliver, University of Notre Dame, for assistance with the Hirshfeld analyses.

## Notes and references

- N. Murugesan, P. W. Glunz, M. S. Bodas, N. D. Yadav and V. Alla, *WO Pat.*, 2017-US34613 2017205709, 2017.
- S. Ahmad, *WO Pat.*, 2015-US18870 2015134699, 2015.
- A. Bahadoor, A. C. Castro, L. K. Chan, G. F. Keaney, M. Nevalainen, V. Nevalainen, S. Peluso, D. A. Snyder and T. T. Tibbitts, *WO Pat.*, 2011-US35141 2011140190, 2011.
- U. Grether, M. Nettekoven, B. Puellmann, S. Roever, M. Rogers-Evans and T. Schulz-Gasch, *WO Pat.*, 2014-EP615272014198592, 2014.
- J. I. Andres-Gil, M. J. Alcazar-Vaca, J. Pastor-Fernandez, W. H. I. M. Drinkenburg, X. J. M. Langlois, J. Oyarzabal-Santamarina and J. A. Vega-Ramiro, *WO Pat.*, 2005-EP56951 2006067139, 2006.
- T. L. Shih, M. R. Candelore, M. A. Cascieri, S.-H. L. Chiu, L. F. Colwell, Jr., L. Deng, W. P. Feeney, M. J. Forrest, G. J. Hom and D. E. MacIntyre, *Bioorg. Med. Chem. Lett.*, 1999, **9**, 1251–1254.
- M. A. J. Duncton, R. B. Murray, G. Park and R. Singh, *Org. Biomol. Chem.*, 2016, **14**, 9343–9347.
- Y. Matsuzaki, Y. Yoshimoto, S. Arimori, S. Kiguchi, T. Harada and F. Iwahashi, *Bioorg. Med. Chem.*, 2020, **28**, 115211.
- G. Theodoridis, F. W. Hotzman, L. W. Scherer, B. A. Smith, J. M. Tymonko and M. J. Wyle, *Pestic. Sci.*, 1990, **30**, 259–274.
- R. D. Clark, *ACS Symp. Ser.*, 1994, **559**, 34–47.
- Y.-P. Luo, L. Lin and G.-F. Yang, *J. Heterocycl. Chem.*, 2007, **44**, 937–943.
- Y.-P. Luo and G.-F. Yang, *Bioorg. Med. Chem.*, 2007, **15**, 1716–1724.
- M.-Y. Jiang, L. Yu, Y.-C. Zhou, J. Jia, X.-J. Si, W.-W. Dong, Z.-F. Tian, J. Zhao and D.-S. Li, *Z. Anorg. Allg. Chem.*, 2020, **646**, 268–274.
- X.-Y. Li, Z. Yin, W.-M. Ma, C. Wang, Y.-N. Yu and Y. Cheng, *Inorg. Chem. Commun.*, 2020, **116**, 107925.
- R. Zhang, D.-X. Meng, F.-Y. Ge, J.-H. Huang, L.-F. Wang, Y.-K. Xv, X.-G. Liu, M.-M. Meng, H. Yan, Z.-Z. Lu, H.-G. Zheng and W. Huang, *Dalton Trans.*, 2020, **49**, 2145–2150.
- P. He, J.-G. Zhang, K. Wang, X. Yin and T.-L. Zhang, *J. Phys. Org. Chem.*, 2016, **29**, 29–34.
- P. He, L. Wu, J.-T. Wu, X. Yin, M. Gozin and J.-G. Zhang, *Dalton Trans.*, 2017, **46**, 8422–8430.
- H. Noeth, K. Burger and W. Beck, *Z. Naturforsch., B: J. Chem. Sci.*, 2011, **66**, 972–974.
- F. Janssens, J. Torremans and P. A. J. Janssen, *J. Med. Chem.*, 1986, **29**, 2290–2297.
- F. Janssens, J. Torremans, M. Janssen, R. A. Stokbroekx, M. Luyckx, P. A. J. Janssen and J. Med, *Chem*, 1985, **28**, 1934–1943.
- A. Santhoshi, P. S. Sadhu, R. Sriram, C. N. S. S. P. Kumar, B. Mahendar, M. Sarangapani and V. J. Rao, *Med. Chem. Res.*, 2013, **22**, 3329–3340.
- A. S. Gundugola, K. L. Chandra, E. M. Perchellet, A. M. Waters, J.-P. H. Perchellet and S. Rayat, *Bioorg. Med. Chem. Lett.*, 2010, **20**, 3920–3924.
- B. Alig, S. Cerezo-Galvez, R. Fischer, A. Koehler, J. J. Hahn, A. Becker, K. Ilg, A. Voerste and D. Portz, *WO Pat.*, 2014-EP62521 2014202510, 2014.
- H. Quast and U. Nahr, *Chem. Ber.*, 1985, **118**, 526–540.
- H. Quast, A. Fuss and U. Nahr, *Chem. Ber.*, 1985, **118**, 2164–2185.
- R. Crockett, A. R. Forrester and R. A. Howie, *Acta Crystallogr., Sect. E: Struct. Rep. Online*, 2003, **59**, o1347–o1348.
- Y. Ohno, Y. Akutsu, M. Arai, M. Tamura, T. Matsunaga and M. Iida, *Acta Crystallogr., Sect. C: Cryst. Struct. Commun.*, 1998, **54**, 1160–1162.
- S. Rayat, O. Alawode and J. Desper, *CrystEngComm*, 2009, **11**, 1892–1898.
- R. Y. Morjan, N. H. Al-Attar, O. S. Abu-Teim, M. Ulrich, A. M. Awadallah, A. M. Mkadmh, A. A. Elmanama, J. Raftery, F. M. Abu-Awwad, Z. J. Yaseen, A. F. Elqidrea and J. M. Gardiner, *Bioorg. Med. Chem. Lett.*, 2015, **25**, 4024–4028.
- L. V. Kudzma, S. A. Severnak, M. J. Benvenga, E. F. Ezell, M. H. Ossipov, V. V. Knight, F. G. Rudo, H. K. Spencer and T. C. Spaulding, *J. Med. Chem.*, 1989, **32**, 2534–2542.
- Y. V. Mel'nikova, L. V. Myznikov, A. V. Dogadina and N. I. Svintsitskaya, *Russ. J. Gen. Chem.*, 2014, **84**, 2160–2166.
- G.-D. Zhang, Z. Wang, X. Yin and J.-G. Zhang, *Z. Anorg. Allg. Chem.*, 2018, **644**, 598–601.
- O. Almarsson and M. J. Zaworotko, *Chem. Commun.*, 2004, 1889–1896.
- N. Shan and M. J. Zaworotko, *Drug Discovery Today*, 2008, **13**, 440–446.
- Y. Li, L.-X. Gao and F.-S. Han, *Chem. Commun.*, 2012, **48**, 2719–2721.
- C.-Y. Liu, Y. Li, J.-Y. Ding, D.-W. Dong and F.-S. Han, *Chem. – Eur. J.*, 2014, **20**, 2373–2381.
- S. Monge, V. Darcos and D. M. Haddleton, *J. Polym. Sci., Part A: Polym. Chem.*, 2004, **42**, 6299–6308.
- S. Y. Moon, T. H. Noh and O.-S. Jung, *CrystEngComm*, 2013, **15**, 3854–3861.
- B. Roldan Cuenya, *Acc. Chem. Res.*, 2013, **46**, 1682–1691.
- L. Wu, Y. Zhang and Y.-G. Ji, *Curr. Org. Chem.*, 2013, **17**, 1288–1302.
- Y. Li, E. Boone and M. A. El-Sayed, *Langmuir*, 2002, **18**, 4921–4925.
- E. M. Zahran, N. M. Bedford, M. A. Nguyen, Y.-J. Chang, B. S. Gupton, R. R. Naik, L. G. Bachas and M. R. Knecht, *J. Am. Chem. Soc.*, 2014, **136**, 32–35.
- Y.-H. Tsai, K. Chanda, Y.-T. Chu, C.-Y. Chiu and M. H. Huang, *Nanoscale*, 2014, **6**, 8704–8709.
- M. J. Frisch, G. W. Trucks, H. B. Schlegel, G. E. Scuseria, M. A. Robb, J. R. Cheeseman, G. Scalmani, V. Barone, G. A. Petersson, H. Nakatsuji, X. Li, M. Caricato, A. Marenich, J. Bloino, B. G. Janesko, R. Gomperts, B. Mennucci, H. P.

Hratchian, J. V. Ortiz, A. F. Izmaylov, J. L. Sonnenberg, D. Williams-Young, F. Ding, F. Lipparini, F. Egidi, J. Goings, B. Peng, A. Petrone, T. Henderson, D. Ranasinghe, V. G. Zakrzewski, J. Gao, N. Rega, G. Zheng, W. Liang, M. Hada, M. Ehara, K. Toyota, R. Fukuda, J. Hasegawa, M. Ishida, T. Nakajima, Y. Honda, O. Kitao, H. Nakai, T. Vreven, K. Throssell, J. A. Montgomery, Jr., J. E. Peralta, F. Ogliaro, M. Bearpark, J. J. Heyd, E. Brothers, K. N. Kudin, V. N. Staroverov, T. Keith, R. Kobayashi, J. Normand, K.

Raghavachari, A. Rendell, J. C. Burant, S. S. Iyengar, J. Tomasi, M. Cossi, J. M. Millam, M. Klene, C. Adamo, R. Cammi, J. W. Ochterski, R. L. Martin, K. Morokuma, O. Farkas, J. B. Foresman and D. J. Fox, *Gaussian 09*, Gaussian, Inc., Wallingford CT, 2016.

45 R. Dennington, T. Keith and J. Millam, *GaussView, Version 5*, Semichem Inc., Shawnee Mission, KS, 2009.

46 M. A. Spackman and D. Jayatilaka, *CrystEngComm*, 2009, **11**, 19–32.